Atmos. Meas. Tech., 10, 1155–1168, 2017
www.atmos-meas-tech.net/10/1155/2017/
doi:10.5194/amt-10-1155-2017

Atmospheric Measurement Techniques
Open Access
EGU

Improved OSIRIS NO_2 retrieval algorithm: description and validation

Christopher E. Sioris[1], Landon A. Rieger[2], Nicholas D. Lloyd[2], Adam E. Bourassa[2], Chris Z. Roth[2], Douglas A. Degenstein[2], Claude Camy-Peyret[3], Klaus Pfeilsticker[4], Gwenaël Berthet[5], Valéry Catoire[5], Florence Goutail[6], Jean-Pierre Pommereau[6], and Chris A. McLinden[1]

[1]Air Quality Research Division, Environment and Climate Change Canada, Toronto, Canada
[2]University of Saskatchewan, Saskatoon, Canada
[3]Institut Pierre Simon Laplace, Paris, France
[4]Institute of Environmental Physics, University of Heidelberg, Heidelberg, Germany
[5]LPC2E, Centre National de la Recherche Scientifique, Université Orléans, Orléans, France
[6]Centre National de la Recherche Scientifique, Guyancourt, France

Correspondence to: Christopher E. Sioris (christopher.sioris@canada.ca)

Received: 23 August 2016 – Discussion started: 10 October 2016
Revised: 8 February 2017 – Accepted: 20 February 2017 – Published: 21 March 2017

Abstract. A new retrieval algorithm for OSIRIS (Optical Spectrograph and Infrared Imager System) nitrogen dioxide (NO_2) profiles is described and validated. The algorithm relies on spectral fitting to obtain slant column densities of NO_2, followed by inversion using an algebraic reconstruction technique and the SaskTran spherical radiative transfer model (RTM) to obtain vertical profiles of local number density. The validation covers different latitudes (tropical to polar), years (2002–2012), all seasons (winter, spring, summer, and autumn), different concentrations of nitrogen dioxide (from denoxified polar vortex to polar summer), a range of solar zenith angles (68.6–90.5°), and altitudes between 10.5 and 39 km, thereby covering the full retrieval range of a typical OSIRIS NO_2 profile. The use of a larger spectral fitting window than used in previous retrievals reduces retrieval uncertainties and the scatter in the retrieved profiles due to noisy radiances. Improvements are also demonstrated through the validation in terms of bias reduction at 15–17 km relative to the OSIRIS operational v3.0 algorithm. The diurnal variation of NO_2 along the line of sight is included in a fully spherical multiple scattering RTM for the first time. Using this forward model with built-in photochemistry, the scatter of the differences relative to the correlative balloon NO_2 profile data is reduced.

1 Introduction

Nitrogen oxides, such as NO and NO_2, are the reactive nitrogen-containing species in the middle atmosphere and are produced mainly from the breakdown of nitrous oxide in the stratosphere (Crutzen, 1971). Oxides of nitrogen dominate ozone loss in the middle stratosphere, whereas in the lower stratosphere they react with oxides of chlorine and bromine, such as ClO and BrO, to reduce the halogen-catalyzed destruction of ozone (Salawitch et al., 2005; Wennberg et al., 1994).

The partitioning between NO and NO_2 depends on several factors such as the local ozone concentration and the photolysis frequency of NO_2. Reactive nitrogen is chemically converted at night to N_2O_5 and, upon hydrolysis, can be further sequestered into unreactive "reservoir" species such as HNO_3. NO_2 increases steadily during daylight hours due to the UV photolysis of N_2O_5 (e.g. Wetzel et al., 2012).

The photochemistry of NO_2, which is particularly rapid near the day–night terminator, leads to horizontal gradients within the field of view, particularly for limb sounders such as OSIRIS (Optical Spectrograph and Infrared Imager System) (Llewellyn et al., 2004) on the Odin satellite or for solar occultation instruments operating in either the UV–visible or mid-infrared (e.g. Kerzenmacher et al., 2008). Besides OSIRIS, other space-borne limb scattering instruments

Table 1. Main features of OSIRIS NO_2 algorithms compared in this work.

	v3.0 operational	"Fast"	1-D, 2-D, 3-D
Wavelength range (nm)	435–451	438–450	435–477
Number of spectral pixels	41	13	107
RTM	LIMBTRAN	SaskTran (1-D)	SaskTran (1-D, 2-D, 3-D)
Inversion scheme	Optimal estimation	MART (0.5 : 0.3 : 0.2)	MART (0.6 : 0.3 : 0.1)
Cloud detection	Yes	No	Yes
NO_2 absorption cross sections	220 K (Vandaele et al., 1998)	(Burrows et al., 1998)	220, 298 K (Vandaele et al., 1998)
Interpolation of fitted cross section to effective T	No	Yes, using local ECMWF temperature at each TH	Yes, using local ECMWF temperature at each TH
Reference	Haley and Brohede (2007)	Bourassa et al. (2011)	This work

that have measured NO_2 vertical profiles include Scanning Imaging Absorption spectrometer for Atmospheric Chartography (SCIAMACHY) (Bovensmann et al., 1999), Solar Mesosphere Explorer (Mount et al., 1984), and Stratospheric Aerosol and Gas Experiment (SAGE) III (Rault et al., 2004; Rault, 2004).

The OSIRIS operational NO_2 retrieval algorithm was developed and validated by Haley and Brohede (2007) and the current version is 3.0. The work of Kerzenmacher et al. (2008) is the only other publication comparing version 3.0 OSIRIS NO_2 data to correlative profile measurements. Earlier versions (e.g. 2.x; Haley et al., 2004) were more thoroughly validated, for example by Brohede et al. (2007). The pseudo-spherical forward model used in the operational OSIRIS NO_2 retrieval algorithm is less accurate than the SaskTran spherical radiative transfer model (RTM) (Bourassa et al., 2008; Zawada et al., 2015) currently used as a forward model in the operational retrieval algorithm for OSIRIS ozone and aerosol extinction data products. Recently, Bourassa et al. (2011) developed an alternative NO_2 algorithm which relied on four wavelengths covering a single NO_2 absorption band. This was later modified to 13 wavelengths covering three adjacent NO_2 bands (438–450 nm) and used to process the entire OSIRIS data record and is referred to here as the "fast" OSIRIS NO_2 product. While the spectral information content is reduced relative to the operational OSIRIS algorithm and the algorithm described below (see Table 1), the "fast" algorithm has two key common elements to the one described herein:

1. The forward model is the successive-orders-of-scattering version of SaskTran.
2. MART (Multiplicative Algebraic Reconstruction Technique) (Degenstein et al., 2009) is used for inversion.

In this work, we provide a detailed description of the new retrieval algorithm whose heritage is the "fast" algorithm (Bourassa et al., 2011) as well as the algorithm developed in a series of papers (Sioris et al., 2003, 2004, 2007). The current algorithm was developed to demonstrate that improved accuracy is possible through the combination of a better forward model and better forward model inputs than used by Sioris et al. (2007) and additional wavelengths longer than those selected by Sioris et al. (2003). The main focus is on the lower stratosphere (and upper troposphere).

We then compare NO_2 profiles retrieved from OSIRIS observations to balloon-borne NO_2 profile measurements during the decade (2002–2012) when dozens of balloon-borne limb measurements were performed. Balloon profiles are chosen for the validation for many reasons, of which the most important is the expected accuracy of these data. The accuracy is due to two main factors: very high signal-to-noise ratio afforded by the luxury of long exposure times (which can be traded for higher vertical and/or spectral resolution) and superior altitude determination, which for balloon-borne limb geometry is due to the sensor being an order of magnitude closer to the tangent point than for satellite limb sounders, thereby reducing the impact of imperfect viewing angle knowledge. Profile measurements from balloons are preferable to those from satellite for the purpose of validation because of their high vertical resolution, generally matching or exceeding the ~ 2 km vertical resolution of OSIRIS NO_2 (e.g. Sioris et al., 2003) (see below). Balloon measurements exploit a greater diversity of methods as in situ techniques are used in addition to remote sensing. Furthermore, one balloon-borne remote sensing technique relies on occultation during balloon ascent/descent, which is not possible for satellite instruments, and provides very accurate altitude registration, offers potentially finer vertical resolution than limb geometry for instruments observing the full solar disk (see Sect. 2.3), and smaller errors due to the neglect of diurnal NO_2 gradients.

2 Method

2.1 Algorithm description and settings

The algorithm is a classic two-step approach of spectral fitting of optical depth spectra with absorption cross sections to determine slant column densities (SCDs), followed by vertical fitting to invert the SCD profile (e.g. Ogawa et al., 1981). This two-step approach is used by many groups (e.g. Pommereau, 1982; Ferlemann et al., 1998; Renard et al., 2000) including some of the balloon remote sensing teams providing data used in this study. The profile is retrieved by iteratively updating it based on MART (see below) such that the simulated NO_2 SCDs agree with the observed ones. A generally appropriate diagram of the algorithm described here appears in the work of Haley et al. (2004).

The first step of the data analysis, namely the spectral fitting, involves a reference spectrum as in Eq. (1) of Sioris et al. (2003). The reference spectrum is the co-addition of spectra at tangent heights (THs) in the 50–70 km range (Sioris et al., 2003). Spectral fitting refers to a multiple linear regression including the following basis functions: a fourth-order closure polynomial which is justified based on an adjusted R^2 test, and temperature-dependent NO_2 (Vandaele et al., 1998) and O_3 (Serdyuchenkov et al., 2014) absolute absorption cross sections interpolated to the temperature (T) of the tangent layer using the European Centre for Medium-Range Weather Forecasting (ECMWF) analysis and convolved with a Gaussian to OSIRIS spectral resolution. Water vapour absorption is neglected despite maximal absorptions of > 0.1 % in the fitting window (434.8–476.7 nm) in the upper troposphere as it is not spectrally correlated with NO_2 absorption over this window and would greatly increase the forward modelling computational burden. SaskTran treats water vapour as a line-by-line absorber assuming a Voigt line shape and spectroscopic parameters from the HITRAN 2008 database (Rothman et al., 2009).

The spectral fitting is exactly the same for observed and simulated normalized radiances. For example, the actual OSIRIS wavelengths and tangent heights are inputs into the simulation and any spectral pixels which are rejected due to radiation hits or detector saturation at the Level 1 processing stage (i.e. observed radiances) are also omitted from the fit of the SaskTran-simulated radiances. The longest wavelength in the fitting window is extended to 476.7 nm, raising the number of spectral pixels to 107, thereby increasing the spectrally integrated signal-to-noise ratio and the penetration of the lower atmosphere relative to both existing OSIRIS NO_2 algorithms mentioned above. Both of these benefits of an extended fitting window have been demonstrated for SCIAMACHY limb scattering (Sioris et al., 2004), but OSIRIS has a glass filter that prevents the detection of higher orders of light reflected off the grating, which was positioned such that the 477–530 nm region is not usable (Warshaw et al., 1996). Thus the 434.8–476.7 nm window is used here and spectral fitting residuals are shown in Fig. 1. Using a discontinuous fitting window that included wavelengths greater than 530 nm is not beneficial. The NO_2 SCD uncertainties are improved relative to those obtained by Sioris et al. (2003) who used a 434.8–449.0 nm fitting window and the "tilt" pseudo-absorber. The improved NO_2 number density precision is illustrated below. The "tilt" basis function is now excluded from the spectral fitting. We also tested an alternative approach of fitting an NO_2 spectral weighting function to the normalized radiances, as is used to fit the ozone absorption signal in nadir reflectance spectra (Coldewey-Egbers et al., 2005) and the spectral fits did not improve significantly.

The retrieval upper altitude limit is defined by the lowest TH in a limb scan for which the NO_2 SCD error is < 100 % for all THs below. This can be as high as 49 km but is typically ~ 40 km and typically a few kilometres higher than the upper altitude of the "fast" NO_2 product. The lower limit of the retrieval is often determined by cloud tops as Odin generally scans the limb into the upper troposphere; cloud-contaminated observations are excluded as they can lead to biases and poor retrieval convergence. Cloud top detection is particularly important for MART since spectra from successive THs immediately below a given altitude are used in a weighted fashion to retrieve the NO_2 number density at that altitude. We assume, for OSIRIS geometry (scattering angles of $90 \pm 30°$), that an observed scene near a cloud top sampled by the ~ 1 km tall instantaneous field of view has larger limb radiance at ~ 810 nm than if it were cloud free. A scene is deemed to be cloudy if the ~ 810 nm radiance scale height is < 2.4139. This threshold is lowered from an overly stringent value of 3.84 (Sioris et al., 2007). The new threshold is chosen to allow NO_2 retrievals (and validation) to extend below 2–3-month old volcanic aerosol layers due to Sarychev Peak and Nabro, two of the eruptions during the OSIRIS mission which led to the largest stratospheric aerosol optical depth.

Algebraic reconstruction techniques have been used to recover the vertical (and along-track) distribution of atmospheric constituents for over 4 decades (Thomas and Donahue, 1972; Fesen and Hays, 1982). Chahine's (1968) relaxation method, used by Sioris et al. (2007) for the retrieval of OSIRIS NO_2 vertical profiles, is a variant of MART in which only the tangent layer is used to retrieve the local number density and is also tested (see Sect. 4). The MART retrieval in this work uses a $0.6 : 0.3 : 0.1$ weighting following the OSIRIS aerosol extinction retrieval (see Eq. 8 of Bourassa et al., 2007). Exactly 15 retrieval iterations are used, which appears to be adequate for most cases and, with MART, does not lead to overfitting. The radiance is summed over five orders of scattering, which is sufficient for non-cloudy cases (Sioris et al., 2004) and also leads to ≤ 6 % errors over the retrieval range for a case with a solar zenith angle (SZA) of 75° with an optically thick ice cloud occupying two altitude levels within the boundary layer. The NO_2 profile is retrieved on a 1 km altitude grid, although the NO_2 vertical resolution remains ~ 2 km, a consequence of the ~ 2 km vertical sam-

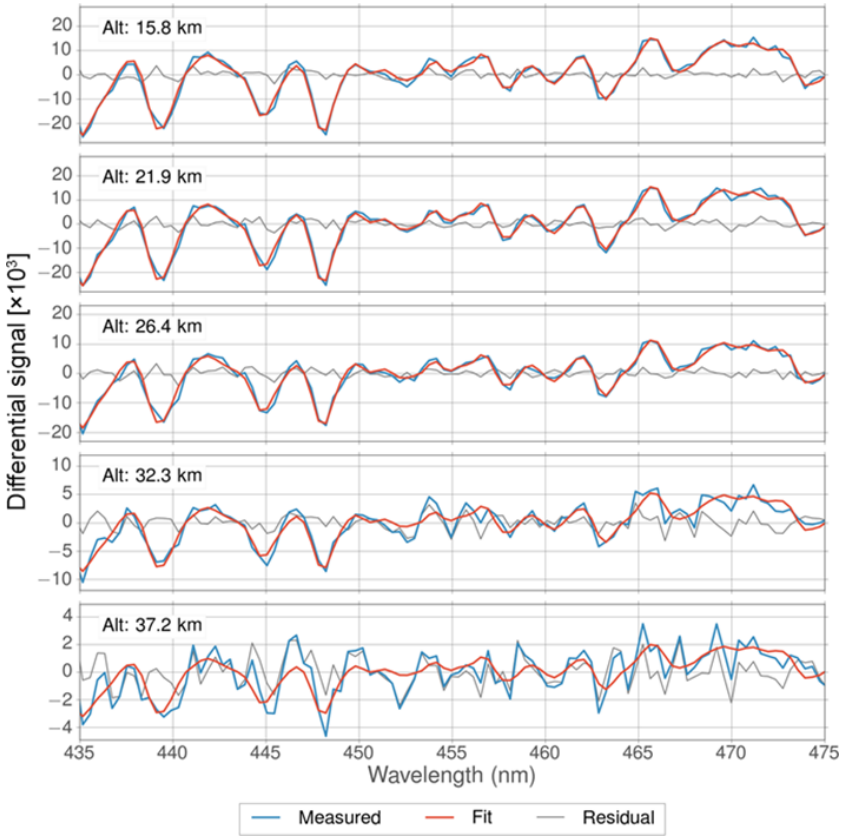

Figure 1. Measured and fitted differential optical depth (DOD) as a function of tangent height ("Alt") in the spectral window used for NO_2 retrieval. The residual is calculated as measured DOD minus fitted DOD.

pling provided by Odin. Above the retrieval range, NO_2 profiles are scaled every iteration using a Chahine-like update based on the highest TH within the retrieval range. Below the retrieval range, the NO_2 profile is assumed to have a constant number density down to the ground, equal to the number density at the lowest retrieved altitude. The air number density profile is from ECMWF. The retrieval uses OSIRIS-retrieved ozone and aerosol extinction profiles (version 5.07, v5.07 hereafter), as well as the 675 nm scene albedo (Bourassa et al., 2007) to provide more realistic forward model inputs into SaskTran.

The NO_2 retrieval uncertainty is obtained by perturbation as described by Sioris et al. (2010), with the NO_2 SCD standard errors and an altitude-independent NO_2 number density perturbation serving as inputs. Profile retrieval including the error calculation using a forward model that neglects diurnal gradients (see Sect. 2.2) takes $\sim$ 5 min on a desktop computer with eight 3.4 GHz processors.

2.2 Modelling diurnal gradients within SaskTran

McLinden et al. (2006) developed the capability to account for diurnal chemical gradients in a pseudo-spherical RTM. The high spatial resolution capability which is required for modelling (horizontal) diurnal gradients of NO_2 within the fully spherical SaskTran RTM is described by Zawada et al. (2015). This capability comes at the price of a large increase in computing time (see also Sect. 3). SaskTran is now capable of modelling radiation fields with the atmosphere varying along the line of sight (LOS) as well as along the incoming solar beam (referred to as "2-D mode" and "3-D mode", respectively, hereafter). The 1-D forward model and associated retrieval (Table 1) completely neglects diurnal gradients in NO_2. In 2-D mode, the atmosphere consists of sectors along the LOS (with 1°, angular resolution) but the diurnal variation of NO_2 along the incoming solar beam is not considered. In 3-D mode, the atmosphere essentially consists of stacked triangular prisms of increasing horizontal extent with increasing distance from the tangent point as illustrated by Zawada et al. (2015) and diurnal gradients are simulated for any light path from its point of entry into the atmosphere to its exit.

To provide realistic diurnal gradients in the atmosphere of the forward model, SaskTran has been linked to the PRATMO stratospheric gas-phase photochemical box model (McLinden et al., 2000). PRATMO is configured to converge to 0.5 % between the start and end of each 1-day run. The default number of time steps per day is 35. The latitudinal and

vertical resolutions are 2.5° and ∼ 2 km, respectively. The atmosphere is aerosol free for photolysis frequency calculations. More details are available in McLinden et al. (2006) and references therein. The accuracy of PRATMO at various altitudes, latitudes, seasons, and SZAs is in evidence in the work of Brohede et al. (2008).

The diurnal variation within the SaskTran atmosphere is then simulated by scaling the NO_2 number density in each sector by the ratio of NO_2 number density in that sector relative to the tangent sector. NO_2 number density is linearly interpolated from the SZAs in PRATMO to the SZAs of the SaskTran sectors based on the cosine of the SZA. The sectors and the vertical grid in SaskTran are defined independently of the PRATMO latitudinal and vertical grid.

Note that the typical horizontal sampling of OSIRIS limb scans of ∼ 5° is too sparse to allow for a tomographic retrieval (Hultgren et al., 2013). A two-dimensional tomographic retrieval of NO_2 from a special set of SCIAMACHY limb scattering measurements with finer horizontal sampling was performed by Puķīte et al. (2008). Their tomographic retrieval provides an alternative approach to account for the diurnal gradient of NO_2 in the orbital plane (i.e. along the LOS).

2.3 Validation approach and datasets

Even though the OSIRIS profiles retrieved with the 2-D and 3-D mode of SaskTran account, to varying degrees, for the diurnal gradients expected for the OSIRIS viewing geometry, photochemical modelling is also required to scale all of the OSIRIS NO_2 profiles to the local time of the balloon measurement. The PRATMO box model is also used for this purpose.

Balloon correlative data are used from the following instruments: Differential Optical Absorption Spectroscopy (DOAS; Butz et al., 2006; Kreycy et al., 2013, and references therein), mini-DOAS (Weidner et al., 2005), Limb Profile Monitor of the Atmosphere (LPMA; Butz et al., 2006), Spectromètre Infra-Rouge d'Absorption par Lasers Embarqués (SPIRALE; Kerzenmacher et al., 2008; Moreau et al., 2005), Système d'Analyse par Observation Zénithale (SAOZ; Pommereau and Piquard, 1994; Wetzel et al., 2007), SAOZ-BrO (Pundt et al., 2002), mini-SAOZ (Vicomte and Pommereau, 2011), MkIV (Toon et al., 2002), and Spectroscopie d'Absorption Lunaire pour l'Observation des Minoritaires Ozone et NO_x – Nacelle 2 (SALOMON-N2) operating in solar occultation mode (Jégou et al., 2013). Table 2 provides information on these correlative datasets. The five balloon-borne instruments not previously used in OSIRIS NO_2 validation are LPMA, mini-DOAS, SPIRALE, SALOMON-N2, and MkIV. DOAS and SAOZ had been used previously (Brohede et al., 2007; Haley et al., 2004; Sioris et al., 2003). SPIRALE, LPMA, and SALOMON-N2 data were obtained from the CNES/CNRS-INSU Ether website (http://www.pole-ether.fr).

Coincidence criteria are within 1000 km (Brohede et al., 2007) and on the same calendar day (using UT time). Only daytime correlative measurements are considered. The closest spatial coincidence is used if located within a 1000 km range. Comparisons between OSIRIS NO_2 and balloon correlative data are performed only down to the lower altitude limit of each profile retrieved with the v3.0 algorithm in an effort to keep the number of balloon-coincident altitudes the same between that algorithm and the algorithm debuting here. The upper limit for validation is determined in all cases by the balloon float altitude.

The best opportunities for validation of a denoxified profile come on 4 and 16 March 2003 in Kiruna, Sweden, when the NO_2 number density measured by LPMA and SAOZ, respectively, did not exceed 10^9 molec cm^{-3} at any altitude. These peak number densities are the lowest in the validation dataset. Note that OSIRIS does not measure in the northern polar region until late February due to a lack of sunlight at ∼ 06:00 and 18:00. NO_2 profiles at southern high latitudes have not been measured by balloon-borne instruments during the OSIRIS mission.

Averaging kernels are not taken into account since the vertical resolution is similar between the NO_2 profiles from most of the selected validation instruments and from the three OSIRIS algorithms, namely the operational v3.0, "fast", and the algorithm described herein. Results from the current algorithm will be treated separately for each of the forward model modes (1-D, 2-D, and 3-D) described in Sect. 2.2.

In Sect. 3, the 1-D profiles used in the validation are those processed by a network of computers (using a SZA cutoff of $< 90°$). The entire OSIRIS data record has now been processed using the 1-D algorithm and is currently available (University of Saskatchewan, 2017). One time-saving approximation is used to process the entire record: multiple scattering (MS) is only calculated at 21 wavelengths corresponding to the peaks and troughs of the NO_2 absorption cross section across the spectral fitting window rather than the entire set of 107 wavelengths. Radiance ratios between multiple scattering and single scattering simulations at these 21 wavelengths are linearly interpolated to the remaining 86 wavelengths, where they are used to scale the single-scattering radiances. The radiance error due to the MS approximation is typically < 0.05 % at all wavelengths and all THs used in the NO_2 retrieval.

3 Results

One difference in the method described above (Sect. 2) compared to previous OSIRIS NO_2 algorithms (e.g. Haley and Brohede, 2007; Bourassa et al., 2011) is the use of spectral information at longer wavelengths, which allows the NO_2 absorption optical depth to be more precisely quantified. Two sources of random error in retrieved NO_2 are shot noise, a consequence of the finite number of electrons generated by

Table 2. Summary of validation data based on OSIRIS coincidences. The minimum relative uncertainty is reported on the native vertical grid. Vertical resolution is quoted or calculated for an altitude of 16 km. The vertical resolution is provided by Butz (2006) for LPMA and DOAS, Weidner et al. (2005) for mini-DOAS, available at http://mark4sun.jpl.nasa.gov/m4data.html for MkIV, and calculated for limb occultation for the SAOZ-type instruments, including SALOMON-N2 (Jégou et al., 2013), assuming vertical resolution equal to the vertical extent of the solar disk at the tangent point. Uncertainties are for a 1 km vertical grid, except for SPIRALE (0.005 km) and mini-DOAS (2 km).

Instrument	Number of coincidences	Relative uncertainty (%)	Vertical resolution (km)	Average lower altitude (km)	Average upper altitude (km)
MkIV	6	2	~ 2	9	38
SPIRALE	4	< 1	0.005	16	33
SALOMON-N2	1	15	2	15	33
DOAS asc	3	5	1.5	9	29
DOAS limb	4	< 1	1.5	13	32
Mini-DOAS	2	4	2	8	29
LPMA asc	1	10	6	10	33
LPMA limb	4	10	5	15	31
Mini-SAOZ	1	4	2	15	29
SAOZ-BrO asc	1	2	1	3	36
SAOZ-BrO SS	1	4	2	22	37
SAOZ asc/desc	9	< 1	1	6	29
SAOZ limb	9	< 1	2	11	29

the detector by impinging limb-scattered photons, as well as radiation hits by energetic particles (e.g. protons) that are not filtered in the Level 1 data. The extended fitting window tends to reduce the susceptibility of the retrieved NO_2 to these noise sources. Using the 1-D forward model described above, the 33 OSIRIS limb scans used in validation are processed with the extended fitting window and the one used in the operational algorithm (Haley and Brohede, 2007). The standard deviation in retrieved NO_2 number density for each set (i.e. fitting window) is calculated over the common altitude range for each of the 33 scans. Natural variability of NO_2 is identical since the same limb scans and altitude ranges are used, so any difference in the standard deviation is due solely to the different spectral fitting windows. Figure 2 (left panel) shows the slight but systematic reduction in NO_2 variability at all altitudes with the extended fitting window. Note that the NO_2 profiles retrieved from the two fitting windows do not have a significant bias (± 1 standard error) between themselves, which points to the self-consistency of NO_2 spectral cross section between the two windows.

Other benefits of the extended fitting window are that the NO_2 retrieval uncertainty is improved by $\sim 20\,\%$ and the upper altitude limit of the retrieval moves slightly higher, as shown in the right panel of Fig. 2 for a sample case. For this tropical case, only at the NO_2 number density minimum at 15.5 km is the current retrieval unable to measure NO_2 with uncertainty of $< 100\,\%$, whereas with the fitting window of the operational algorithm the measurements are below the lower detection limit between 11.5 and 17.5 km and at 7.5 km (Fig. 2). The significant upper tropospheric NO_2 enhancement at ~ 10 km is also observed by the mini-SAOZ (not shown).

Figure 3 shows that the impact of the different forward model modes: the 1-D retrieval overestimates NO_2 by 29 % relative to the one using the 3-D forward model mode at 17.5 km. Note that relative diurnal gradients are expected to be largest below 18 km. The overestimate for this sample case is due to the larger NO_2 concentrations that are present on the far side of the limb (yet neglected by a 1-D model) for a SZA (86.6°) that is small enough to allow significant far side contribution to the radiance. The increasing NO_2 gradient toward the far side of the limb occurs because of the decreasing photolysis frequency of NO_2 with increasing SZA. The retrieval using the 2-D forward model underestimates slightly since the slightly lower NO_2 concentrations along the incoming solar beam are not included in that model version. The 3-D forward model clearly reduces the bias vs. SAOZ relative to the 1-D forward model at altitudes below 18 km. This improved precision is demonstrated below for a large ensemble of profiles by contrasting the correlation of the retrievals using the 1-D and 2-D forward model modes and the standard error of the biases relative to coincident balloon data. The slightly lower NO_2 number density at 20.5 km retrieved with the 1-D forward model (Fig. 3) is probably

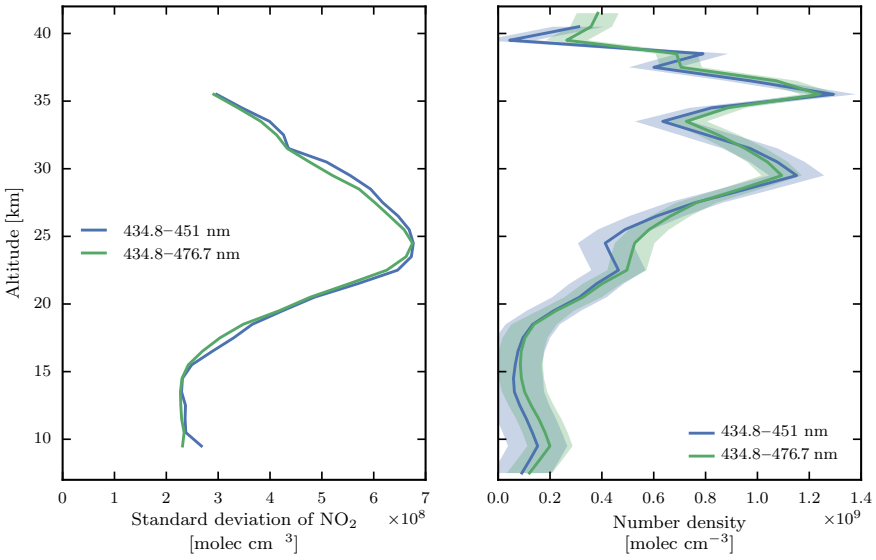

Figure 2. Left: comparison of the standard deviation of the NO_2 number density profiles retrieved with the new algorithm using the default window (435–477 nm, green) vs. the fitting window used in the OSIRIS v3.0 operational algorithm (Haley and Brohede, 2007; blue). Right: comparison of a single NO_2 profile retrieved from scan 20 of orbit 60346 with the algorithm described above using the default window (435–477 nm) vs. the fitting window used in the OSIRIS v3.0 operational algorithm. The retrieval uncertainty for each profile is bound by a shaded area of matching colour.

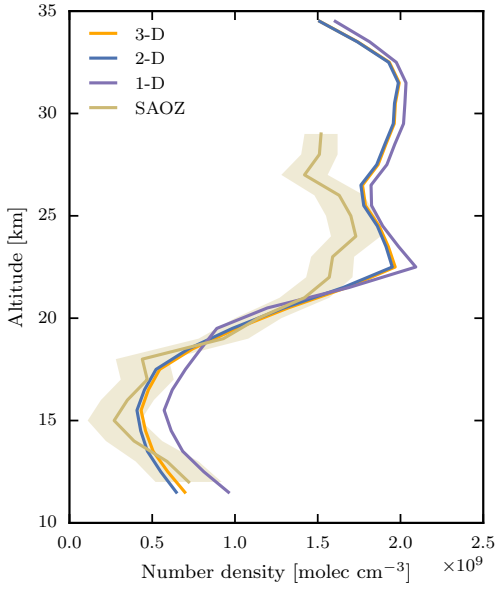

Figure 3. NO_2 profile retrieved from scan 44 of orbit 16011 using the 1-D, 2-D, and 3-D retrievals, all converted to sunset (tangent point SZA = 90°), the local time of coincident SAOZ measurements at Bauru (22.35° S, 49.03° W). OSIRIS is on the day side with SZA = 86.6° (p.m.) and an azimuth difference angle of 99° such that the far side of the limb is closer to the terminator.

a minor oscillation due to an overestimation immediately above at 22.5 km where a secondary NO_2 number density peak is observed by OSIRIS.

In order to compare the various OSIRIS NO_2 products to the balloon correlative data, all profiles are linearly interpolated onto a 1 km grid (12.0–39.0 km) commonly used in the balloon data (see Supplement). The "fast" product tends to be limited in its vertical range at both extremes of the profile, relative not only to the other OSIRIS NO_2 products but also to the coincident balloon profiles, and also the "fast" retrieval is not available for some coincidences (Fig. 4). The sample size is ≥ 20 between 13 and 31 km for all OSIRIS NO_2 products and thus, hereafter, the validation discussion focusses on this altitude range.

The v3.0 operational OSIRIS NO_2 has proven to be of high quality in the 15–42 km range from previous satellite intercomparisons (e.g. Haley and Brohede, 2007) and the same can also be inferred for the upper troposphere from the ability to detect small lightning-generated NO_2 enhancements with the expected latitudinal and longitudinal distribution (e.g. Sioris et al., 2007). Thus, in Fig. 5, we examine the standard error of the coincident profiles for OSIRIS and balloon data to compare the variability of each dataset, similar to Kerzenmacher et al. (2008). The upper altitude limit of the data obtained from balloons launched by CNES (Centre National d'Études Spatiales) is 31 ± 2 km (Table 2). This excludes MkIV and SAOZ-BrO. From 31 down to 28 km, the balloon-borne NO_2 profiles show more scatter than any of the OSIRIS data products. This is likely due to the need to assume the NO_2 vertical distribution above float altitude for the remote sensors, which is particularly problematic in the tropics where the NO_2 profile typically peaks at a higher altitude than for the extratropics. A second factor is the smaller ab-

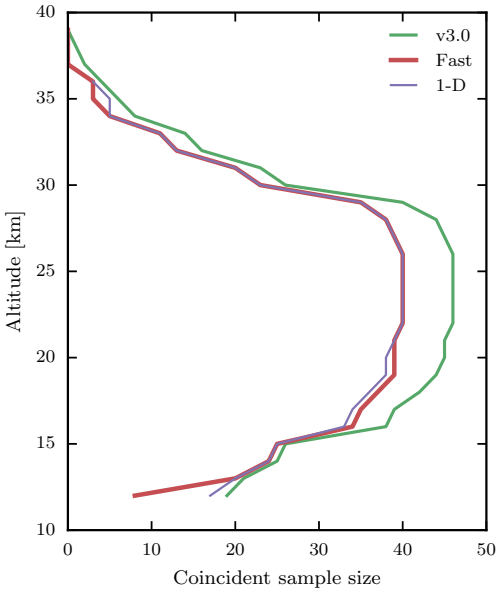

Figure 4. Sample size of coincident balloon data vs. altitude and as a function of retrieval algorithm. Sample size vs. height for 2-D mode is identical to that for 1-D mode.

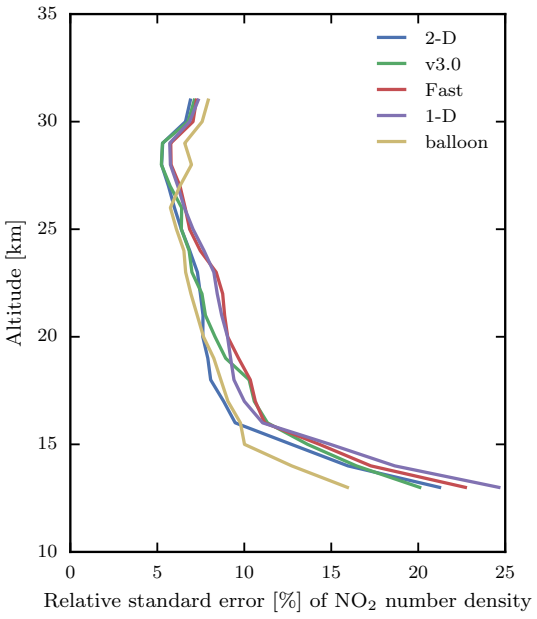

Figure 5. Relative standard error of coincident NO_2 profiles. Note that OSIRIS profiles have been scaled to various local times of the balloon measurements, which adds random error to the OSIRIS profiles due to random variations between the photochemical model atmosphere and the true atmosphere.

sorption signal for the remotely sensing balloon instruments due to the short path lengths when observing altitudes near float. Below 16 km, the balloon data clearly exhibit less scatter than OSIRIS, thereby quantitatively supporting the choice of balloon validation data for reasons discussed in Sect. 1. Kerzenmacher et al. (2008) show that this is not true for NO_2 at $\sim$ 15 km measured by the ACE (Atmospheric Chemistry Experiment) satellite instruments relative to OSIRIS v3.0 NO_2. Between the three OSIRIS products, "fast" exhibits the largest scatter at all altitudes, whereas the 2-D algorithm described here offers noticeably less scatter between 15 and 20 km as compared to the v3.0 product. The 3-D algorithm takes 1.5 h to retrieve a profile on the computer specified above and thus the entire set of balloon-coincident OSIRIS limb scans was not processed. The 2-D algorithm takes half of the processing time of the 3-D algorithm.

To determine whether OSIRIS NO_2 is biased relative to the balloon data, we studied medians and means of individual profile differences over all coincidences (as a function of altitude). These results are shown in Figs. 6 and 7. It is clear that all of the OSIRIS NO_2 algorithms have a statistically significant bias near the NO_2 peak (typically $\sim$ 30 km). This overestimate near the peak is similar to the overestimate by OSIRIS v3.0 relative to ACE Fourier transform spectrometer and MAESTRO (Measurements of Aerosol Extinction in the Stratosphere and Troposphere Retrieved by Occultation), which coincided with the NO_2 peak altitude. Local biases were +17 and 14 %, respectively (Kerzenmacher et al., 2008). Haley and Brohede (2007) found no such overestimate at the peak vs. SAGE III and POAM (Polar Ozone and Aerosol Measurement) III, but a similar positive bias near $\sim$ 28 km vs. HALOE (Halogen Occultation Experiment). The "fast" product has the largest overestimate at the peak, averaging $\sim$ 20 % with a sharp gradient in its bias, such that, at 18 km, there is a statistically significant $\sim$ 20 % underestimate. The retrieved profiles using the 2-D retrieval described above have a similar bias profile shape with "fast" (Figs. 6, 7) but are of smaller amplitude, with a $\sim$ +10 % typical median bias at the number density peak for the 2-D retrieval and a $\sim$ 10 % underestimation at 18 km, which is statistically insignificant in terms of the median bias (Fig. 6). The bias of the v3.0 product is similar to the alternative OSIRIS NO_2 products above 20 km, but between 15 and 17 km there is a significant positive bias using both central tendency statistics (Figs. 6, 7). In contrast to "fast" and v3.0 products, there are no altitudes in the lower stratosphere (below 24 km) with statistically significant average and median biases for the 1-D and 2-D products. This conclusion is not sensitive to the use of the MS approximation used for the 1-D product (see Sect. 2.3) (not shown).

While Figs. 6 and 7 address the systematic errors of the various OSIRIS products, it is also important to consider the precision of these data since a product whose biases in individual profiles average to zero could still fail to adequately capture the variability. This is potentially a greater concern for the v3.0 product since it relies slightly on a priori NO_2 and vertically smooths the retrieved NO_2 when measurement precision is lacking. However, Haley and Brohede (2007) and Haley et al. (2004) show that these are very minor concerns

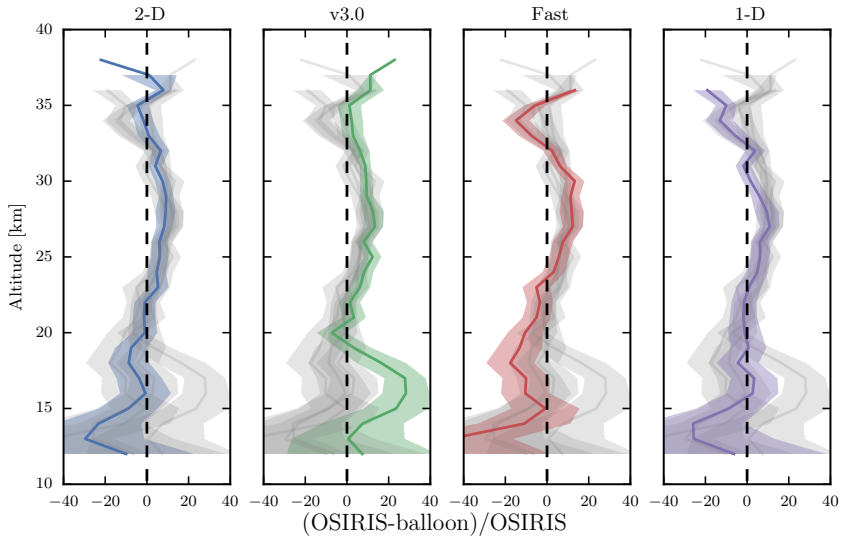

Figure 6. Median of individual biases vs. balloon data. The error bar shows ±1 standard error of the median NO_2 bias profile. The median and standard error of the individual biases are converted to relative quantities by dividing by the corresponding median OSIRIS NO_2 profile (scaled to balloon local time). The relative median bias profiles for the other three algorithms are shown in grey for comparison.

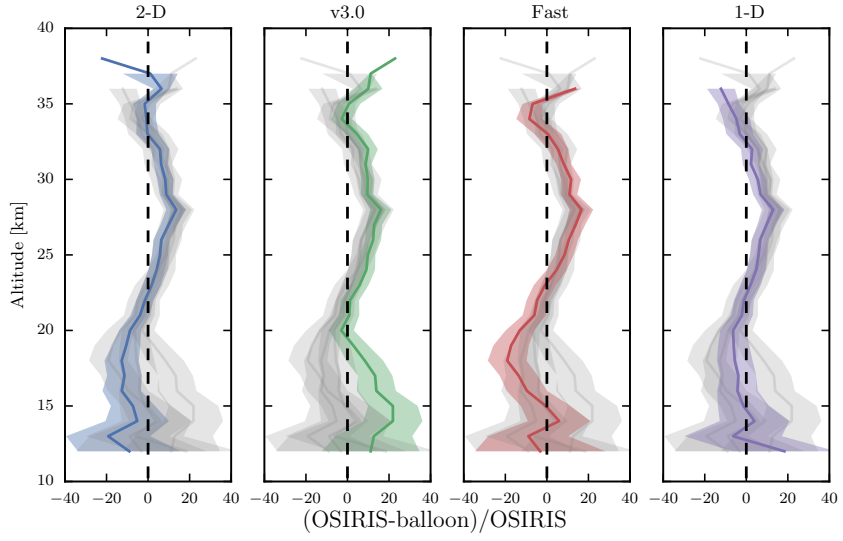

Figure 7. Same as Fig. 6, but the bias is an average over individual differences between OSIRIS and balloon correlative data. The average and standard error of the individual biases are converted to relative quantities by dividing by the corresponding average OSIRIS NO_2 profile (scaled to balloon local time).

as the measurement response and vertical resolution do not deteriorate significantly down to an altitude of 12 km. Figure 8 shows that the v3.0 product captures the variability of the balloon measurements down to ∼ 22 km as well as the 2-D and 1-D products and better than "fast" NO_2, but then has larger scatter below 20 km than the 2-D and "fast" products. The "fast" retrieval benefits from more accurate forward modelling than the v3.0 algorithm. The reduced scatter for the "fast" NO_2 product in the lower stratosphere is unlikely to be a difference between inversion approaches (MART vs. the optimal estimation approach used in the v3.0 algorithm) as discussed above. The new product also may have an edge over the v3.0 product by virtue of using SaskTran as its forward model. For the 2-D mode, there is also the specific benefit of the forward model accounting for diurnal gradients in NO_2. This can be seen clearly between 13 and 16 km where profiles retrieved with the 2-D forward model mode tend to be more precise than those retrieved using the 1-D mode due to this built-in photochemical modelling capability. This confirms the better precision of the 2-D retrieval suggested by Fig. 3 and is only expected for large SZAs (McLinden et al., 2006). Note that errors due to the neglect of diurnally

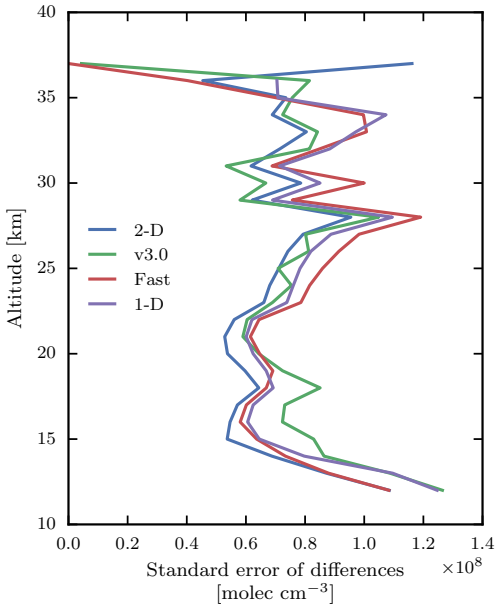

Figure 8. Standard error of the individual biases relative to balloon correlative data for different OSIRIS NO_2 products. The curves here correspond to the half-widths of the error bars in Figs. 6 and 7.

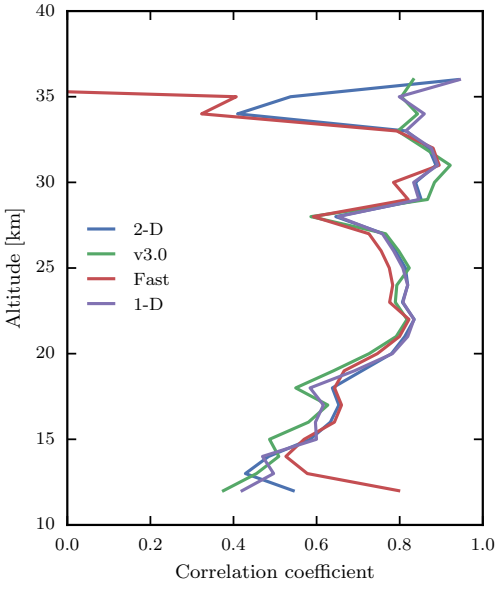

Figure 9. Correlation between various OSIRIS NO_2 products and the balloon validation dataset.

varying chemical gradients can alternate in sign depending on the viewing geometry (McLinden et al., 2006; Brohede et al., 2007), so mean or median biases may not be significantly affected by switching from the 1-D to the 2-D RTM mode (Figs. 6, 7), even though the standard error of the individual biases is reduced (Fig. 8).

Correlation can be used as an alternative statistic to verify whether an OSIRIS product captures the variability observed by coincident balloon data. It is different from the standard error statistic used in Fig. 8 since multiplicative or additive biases do not affect the correlation but do affect the standard error of the individual biases. The correlation is calculated over the 46 coincident balloon profiles at each available altitude (Fig. 4). Figure 9 shows a general decrease in correlation between OSIRIS and coincident balloon data with decreasing altitude. There is higher correlation with balloon NO_2 data for the 2-D mode retrieval over the 1-D mode retrieval at the lowest altitudes, consistent with Fig. 3. The correlation of the v3.0 product is comparable with the 1-D and 2-D mode products down to the lowest validated altitudes, whereas the "fast" product has generally lower correlations above 22 km than the OSIRIS NO_2 products relying on spectral fitting.

Finally, since the coverage of balloon is limited to latitudes north of −22° S, Fig. 10 is included to illustrate the climatological (2001–2015) vertical, meridional, and seasonal variation of stratospheric NO_2 volume mixing ratio in the Southern Hemisphere during austral spring and summer. For each NO_2 vertical profile, the conversion to mixing ratio uses the local air density profile from the ECMWF analysis.

4 Discussion

Next, we review and discuss the sensitivity of the retrieval to forward model parameters. There is a slight sensitivity of the retrieved NO_2 to changes in aerosol extinction. Previous sensitivity studies (Sioris et al., 2003; Haley et al., 2004) are consistent with the current findings. The scene albedo in the visible can vary from < 0.03 for calm ocean to almost unity for fresh snow, although the NO_2 retrieval is, by design, insensitive to surface albedo by virtue of the high-TH normalization of the radiance spectra (Sioris et al., 2003). Use of the retrieved scene albedo (instead of the default value of 0.3) and of the v5.07 aerosol extinction profile further reduce these sensitivities. Finally, use of OSIRIS-observed (v5.07) ozone instead of the default ozone climatology in SaskTran (McPeters et al., 2007) is expected to have a minor impact on retrieved NO_2 via errors in modelling the atmospheric extinction based on Sioris et al. (2007).

With a method that involves simulating spectra at high THs for the purpose of normalizing radiances simulated for THs within the retrieval range, the forward model must accurately compute the radiance over a large range of THs. The NO_2 retrieval error due to the pseudo-spherical approximation is expected to have its largest impact at low altitudes because of the vertical gradient in pseudo-spherical RTM errors (Griffioen and Oikarinen, 2000). At the top of the retrieval range (40 km), the error due to this approximation is cancelled by the use of the high altitude reference.

While not included in Figs. 5–9, Chahine's relaxation method tends to produce sharper extrema in the retrieved NO_2 profile than MART that tend to be slightly displaced vertically from those in the balloon data. This may stem from

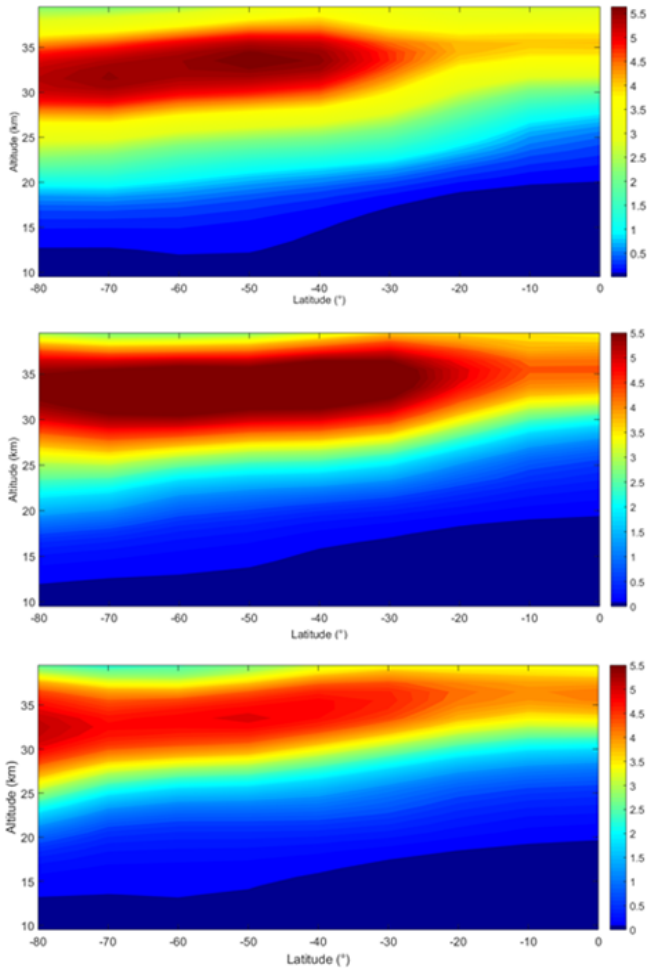

Figure 10. Climatological map of zonal mean NO_2 volume mixing ratio (ppb) with 10° latitudinal binning and 1 km vertical binning centred at altitudes between 9.5 and 39.5 km for November (2001–2014, top), January (2002–2014, middle), and March (2002–2014, bottom).

the coincidence criterion of 1000 km in distance, but it may also relate to the ∼2 km vertical sampling of OSIRIS and the 1 km altitude grid used for the retrieval. If the vertical grid of the retrieval is finer than the vertical sampling, a vertically narrow layer at 19 km, for example, would be retrieved as peaking at 18 km when the available radiance spectra are measured at THs of 18 and 20 km. The comparison of MART and Chahine inversion approaches is worth revisiting with the 1 km vertical sampling offered by the Ozone Mapping Profiler Suite (Jaross et al., 2014).

In order to rigorously validate this new retrieval algorithm in the upper troposphere, tropospheric chemistry must be added to the photochemical model used to scale the OSIRIS observations to balloon local time. The reaction of NO_2 with the hydroxyl radical to form HNO_3 drives the diurnal variation of tropospheric NO_2 more than N_2O_5 photolysis (Boersma et al., 2009). Accurate knowledge of the seasonal variation of the OH concentration is required for modelling the diurnal variation of upper tropospheric NO_2.

5 Conclusions

Profiles of NO_2 retrieved from OSIRIS have been improved in terms of reduced bias and scatter vs. the current v3.0 operational algorithm in the lower stratosphere (e.g. 15 km) as determined using highly accurate balloon measurements as truth. The median bias is within $\sim\pm10$ % between 14 and 37 km.

The benefits of spectral fitting and extending the fitting window to longer wavelengths are evident at the highest altitudes where the photoelectron shot noise tends to be large relative to the NO_2 absorption signal, as well as at the lowest altitudes where the retrieved profile shape is largely driven by small differences in NO_2 SCDs obtained from spectra at adjacent tangent heights. Algorithms that exploit the richness of the NO_2 absorption spectrum are shown to better capture the mid-stratospheric variability of this key constituent. The use of a fully spherical forward model is an important advantage, particularly at lower altitudes since, while the pseudo-spherical RTM errors are largest at the top of the retrieval range, the largest NO_2 retrieval errors due to the use of a pseudo-spherical RTM occur at low altitudes because a high tangent height reference is used in the retrieval.

A model capable of modelling diurnal gradients in NO_2 also helps to improve the precision of the retrieved number density profile, particularly at the lowest altitudes where the horizontal gradients in NO_2 are sharpest and where the radiance is predominantly from the near side of the limb.

Data availability. The OSIRIS NO_2 data record is currently available at ftp://odin-osiris.usask.ca/Level2/no2_v6.0.2 following registration.

The Supplement related to this article is available online at doi:10.5194/amt-10-1155-2017-supplement.

Competing interests. The authors declare that they have no conflict of interest.

Acknowledgements. This work was supported by Environment and Climate Change Canada through a contribution to the University of Saskatchewan. The OSIRIS project is supported by the Canadian Space Agency. Daniel Zawada (University of Saskatchewan) is acknowledged for helpful discussions regarding the high spatial resolution version of the SaskTran model. Alexei Rozanov (University of Bremen) is acknowledged for sharing his experience with the weighting-function DOAS method. Patrick Sheese (University

of Toronto) provided the idea to use correlation as a statistic for validation. SALOMON-N2, SPIRALE, SAOZ, mini-SAOZ, and LPMA data were obtained from CNES/CNRS-INSU Ether website.

Edited by: M. Weber
Reviewed by: two anonymous referees

References

Boersma, K. F., Jacob, D. J., Trainic, M., Rudich, Y., DeSmedt, I., Dirksen, R., and Eskes, H. J.: Validation of urban NO_2 concentrations and their diurnal and seasonal variations observed from the SCIAMACHY and OMI sensors using in situ surface measurements in Israeli cities, Atmos. Chem. Phys., 9, 3867–3879, doi:10.5194/acp-9-3867-2009, 2009.

Bourassa, A. E., Degenstein, D. A., Gattinger, R. L., and Llewellyn, E. J.: Stratospheric aerosol retrieval with optical spectrograph and infrared imaging system limb scatter measurements, J. Geophys. Res., 112, D10217, doi:10.1029/2006JD008079, 2007.

Bourassa, A. E., Degenstein, D. A., and Llewellyn, E. J.: SaskTran: A spherical geometry radiative transfer code for efficient estimation of limb scattered sunlight, J. Quant. Spectrosc. Ra., 109, 52–73, 2008.

Bourassa, A. E., McLinden, C. A., Sioris, C. E., Brohede, S., Bathgate, A. F., Llewellyn, E. J., and Degenstein, D. A.: Fast NO_2 retrievals from Odin-OSIRIS limb scatter measurements, Atmos. Meas. Tech., 4, 965–972, doi:10.5194/amt-4-965-2011, 2011.

Bovensmann, H., Burrows, J. P., Buchwitz, M., Frerick, J., Noël, S., Rozanov, V. V., Chance, K. V., and Goede, A. P. H.: SCIAMACHY: Mission objectives and measurement modes, J. Atmos. Sci., 56, 127–150, 1999.

Brohede, S., McLinden, C. A., Urban, J., Haley, C. S., Jonsson, A. I., and Murtagh, D.: Odin stratospheric proxy NO_y measurements and climatology, Atmos. Chem. Phys., 8, 5731–5754, doi:10.5194/acp-8-5731-2008, 2008.

Brohede, S. M., Haley, C. S., McLinden, C. A., Sioris, C. E., Murtagh, D. P., Petelina, S. V., Llewellyn, E. J., Bazureau, A., Goutail, F., Randall, C. E., Lumpe, J. D., Taha, G., Thomason, L. W., and Gordley, L. L.: Validation of Odin/OSIRIS stratospheric NO_2 profiles, J. Geophys. Res., 112, D07310, doi:10.1029/2006JD007586, 2007.

Burrows, J. P., Dehn, A., Deters, B., Himmelmann, S., Richter, A., Voigt, S., and Orphal, J.: Atmospheric remote-sensing reference data from GOME: 1. Temperature-dependent absorption cross-sections of NO_2 in the 231–794 nm range, J. Quant. Spectrosc. Ra., 60, 1025–1031, 1998.

Butz, A.: Case studies of stratospheric nitrogen, chlorine and iodine photochemistry based on balloon borne UV/visible and IR absorption spectroscopy, PhD thesis, Université Paris 6, Paris, 254 pp., 2006.

Butz, A., Bösch, H., Camy-Peyret, C., Chipperfield, M., Dorf, M., Dufour, G., Grunow, K., Jeseck, P., Kühl, S., Payan, S., Pepin, I., Pukite, J., Rozanov, A., von Savigny, C., Sioris, C., Wagner, T., Weidner, F., and Pfeilsticker, K.: Inter-comparison of stratospheric O_3 and NO_2 abundances retrieved from balloon borne direct sun observations and Envisat/SCIAMACHY limb measurements, Atmos. Chem. Phys., 6, 1293–1314, doi:10.5194/acp-6-1293-2006, 2006.

Chahine, M. T.: Determination of the temperature profile in an atmosphere from its outgoing radiance, J. Opt. Soc. Am., 58, 1634–1637, 1968.

Coldewey-Egbers, M., Weber, M., Lamsal, L. N., de Beek, R., Buchwitz, M., and Burrows, J. P.: Total ozone retrieval from GOME UV spectral data using the weighting function DOAS approach, Atmos. Chem. Phys., 5, 1015–1025, doi:10.5194/acp-5-1015-2005, 2005.

Crutzen, P. J.: Ozone production rates in an oxygen-hydrogen-nitrogen oxide atmosphere, J. Geophys. Res., 76, 7311–7327, 1971.

Degenstein, D. A., Bourassa, A. E., Roth, C. Z., and Llewellyn, E. J.: Limb scatter ozone retrieval from 10 to 60 km using a multiplicative algebraic reconstruction technique, Atmos. Chem. Phys., 9, 6521–6529, doi:10.5194/acp-9-6521-2009, 2009.

Ferlemann, F., Camy-Peyret, C., Fitzenberger, R., Harder, H., Hawat, T., Osterkamp, H., Schneider, M., Perner, D., Platt, U., Vradelis, P., and Pfeilsticker, K.: Stratospheric BrO profiles measured at different latitudes and seasons: Instrument description, spectral analysis and profile retrieval, Geophys. Res. Lett., 25, 3847–3850, 1998.

Fesen, C. G. and Hays, P. B.: Two-dimensional inversion technique for satellite airglow data, Appl. Optics, 21, 3784–3791, 1982.

Griffioen, E. and Oikarinen, L.: LIMBTRAN: A pseudo three-dimensional radiative transfer model for the limb-viewing imager OSIRIS on the ODIN satellite, J. Geophys. Res., 105, 29717–29730, 2000.

Haley, C. S. and Brohede, S. M.: Status of the Odin/OSIRIS stratospheric products O_3 and NO_2 data products, Can J. Phys., 85, 1177–1194, 2007.

Haley, C. S., Brohede, S. M., Sioris, C. E., Griffioen, E., Murtagh, D. P., McDade, I. C., Eriksson, P., Llewellyn, E. J., Bazureau, A., and Goutail, F.: Retrieval of stratospheric O_3 and NO_2 profiles from Odin Optical Spectrograph and Infrared Imager System (OSIRIS) limb-scattered sunlight measurements, J. Geophys. Res., 109, D16303, doi:10.1029/2004JD004588, 2004.

Hultgren, K., Gumbel, J., Degenstein, D., Bourassa, A., Lloyd, N., and Stegman, J.: First simultaneous retrievals of horizontal and vertical structures of Polar Mesospheric Clouds from Odin/OSIRIS tomography, J. Atmos. Sol.-Terr. Phy., 104, 213–223, 2013.

Jaross, G., Bhartia, P. K., Chen, G., Kowitt, M., Haken, M., Chen, Z., Xu, P., Warner, J., and Kelly, T.: OMPS Limb Profiler instrument performance assessment, J. Geophys. Res.-Atmos., 119, 4399–4412, doi:10.1002/2013JD020482, 2014.

Jégou, F., Berthet, G., Brogniez, C., Renard, J.-B., François, P., Haywood, J. M., Jones, A., Bourgeois, Q., Lurton, T., Auriol, F., Godin-Beekmann, S., Guimbaud, C., Krysztofiak, G., Gaubicher, B., Chartier, M., Clarisse, L., Clerbaux, C., Balois, J. Y., Verwaerde, C., and Daugeron, D.: Stratospheric aerosols from the Sarychev volcano eruption in the 2009 Arctic summer, Atmos. Chem. Phys., 13, 6533–6552, doi:10.5194/acp-13-6533-2013, 2013.

Kerzenmacher, T., Wolff, M. A., Strong, K., Dupuy, E., Walker, K. A., Amekudzi, L. K., Batchelor, R. L., Bernath, P. F., Berthet, G., Blumenstock, T., Boone, C. D., Bramstedt, K., Brogniez, C., Brohede, S., Burrows, J. P., Catoire, V., Dodion, J., Drummond, J. R., Dufour, D. G., Funke, B., Fussen, D., Goutail, F., Griffith, D. W. T., Haley, C. S., Hendrick, F., Höpfner, M., Huret, N.,

Jones, N., Kar, J., Kramer, I., Llewellyn, E. J., López-Puertas, M., Manney, G., McElroy, C. T., McLinden, C. A., Melo, S., Mikuteit, S., Murtagh, D., Nichitiu, F., Notholt, J., Nowlan, C., Piccolo, C., Pommereau, J.-P., Randall, C., Raspollini, P., Ridolfi, M., Richter, A., Schneider, M., Schrems, O., Silicani, M., Stiller, G. P., Taylor, J., Tétard, C., Toohey, M., Vanhellemont, F., Warneke, T., Zawodny, J. M., and Zou, J.: Validation of NO_2 and NO from the Atmospheric Chemistry Experiment (ACE), Atmos. Chem. Phys., 8, 5801–5841, doi:10.5194/acp-8-5801-2008, 2008.

Kreycy, S., Camy-Peyret, C., Chipperfield, M. P., Dorf, M., Feng, W., Hossaini, R., Kritten, L., Werner, B., and Pfeilsticker, K.: Atmospheric test of the $J(BrONO_2)/k\mathrm{BrO} + NO_2$ ratio: implications for total stratospheric Bry and bromine-mediated ozone loss, Atmos. Chem. Phys., 13, 6263–6274, doi:10.5194/acp-13-6263-2013, 2013.

Llewellyn, E. J., Lloyd, N. D., Degenstein, D. A., Gattinger, R. L., Petelina, S. V., Bourassa, A. E., Wiensz, J. T., Ivanov, E. V., McDade, I. C., Solheim, B. H., McConnell, J. C., Haley, C. S., von Savigny, C., Sioris, C. E., McLinden, C. A., Griffioen, E., Kaminski, J., Evans, W. F., Puckrin, E., Strong, K., Wehrle, V., Hum, R. H., Kendall, D. J. W., Matsushita, J., Murtagh, D. P., Brohede, S., Stegman, J., Witt, G., Barnes, G., Payne, W. F., Piché, L., Smith, K., Warshaw, G., Deslauniers, D.-L., Marchand, P., Richardson, E. H., King, R. A., Wevers, I., McCreath, W., Kyrölä, E., Oikarinen, L., Leppelmeier, G. W., Auvinen, H., Mégie, G., Hauchecorne, A., Lefèvre, F., de La Nöe, J., Ricaud, P., Frisk, U., Sjoberg, F., von Schéele, F., and Nordh, L.: The OSIRIS instrument on the Odin spacecraft, Can. J. Phys., 82, 411–422, 2004.

McLinden, C. A., Olsen, S. C., Hannegan, B. J., Wild, O., Prather, M. J., and Sundet, J.: Stratospheric ozone in 3-D Models: A simple chemistry and the cross-tropopause flux, J. Geophys. Res., 105, 14653–14665, 2000.

McLinden, C. A., Haley, C. S., and Sioris, C. E.: Diurnal effects in limb scatter observations, J. Geophys. Res., 111, D14302, doi:10.1029/2005JD006628, 2006.

McPeters, R. D., Labow, G. J., and Logan, J. A.: Ozone climatological profiles for satellite retrieval algorithms, J. Geophys. Res., 112, D05308, doi:10.1029/2005JD006823, 2007.

Moreau, G., Robert, C., Catoire, V., Chartier, M., Camy-Peyret, C., Huret, N., Pirre, M., Pomathiod, L., and Chalumeau, G.: SPIRALE: a multispecies *in situ* balloonborne instrument with six tunable diode laser spectrometers, Appl. Optics, 44, 5972–5989, 2005.

Mount, G. H., Rusch, D. W., Zawodny, J. M., Barth, C. A., and Noxon, J. F.: Measurements of stratospheric NO_2 from the Solar Mesosphere Explorer satellite. 1. An overview of the results, J. Geophys. Res., 89, 1327–1340, doi:10.1029/JD089iD01p01327, 1984.

Ogawa, T., Shibasaki, K., and Suzuki, K.: Balloon observation of the stratospheric NO_2 profile by visible absorption spectroscopy, J. Meteorol. Soc. Jpn., 59, 410–415, 1981.

Pommereau, J.-P.: Observation of NO_2 diurnal variation in the stratosphere, Geophys. Res. Lett., 9, 850–853, 1982.

Pommereau, J.-P. and Piquard, J.: Ozone and nitrogen dioxide vertical distributions by uv-visible solar occultation from balloons, Geophys. Res. Lett., 21, 1227–1230, 1994.

Puķīte, J., Kühl, S., Deutschmann, T., Platt, U., and Wagner, T.: Accounting for the effect of horizontal gradients in limb measurements of scattered sunlight, Atmos. Chem. Phys., 8, 3045–3060, doi:10.5194/acp-8-3045-2008, 2008.

Pundt, I., Pommereau, J.-P., Chipperfield, M. P., Van Roozendael, M., and Goutail, F.: Climatology of the stratospheric BrO vertical distribution by balloon-borne UV–visible spectrometry, J. Geophys. Res., 107, 4806, doi:10.1029/2002JD002230, 2002.

Rault, D. F.: Ozone, NO_2 and aerosol retrieval from SAGE III limb scatter measurements, Proc. SPIE, 5571, 205–216, doi:10.1117/12.564899, 2004.

Rault, D. F., Loughman, R., and Sioris, C: Retrieval of atmospheric ozone and nitrogen dioxide vertical distribution from SAGE III limb scattering measurements, Proc. SPIE, 5235, 298–309, doi:10.1117/12.509827, 2004.

Renard, J.-B., Chartier, M., Robert, C., Chalumeau, G., Berthet, G., Pirre, M., Pommereau, J.-P., and Goutail, F.: SALOMON: a new, light balloonborne UV–visible spectrometer for nighttime observations of stratospheric trace-gas species, Appl. Optics, 39, 386–392, 2000.

Rothman, L. S., Gordon, I. E., Barbe, A., Benner, D. C., Bernath, P. F., Birk, M., Boudon, V., Brown, L. R., Campargue, A., Champion, J.-P., Chance, K., Coudert, L. H., Dana, V., Devi, V. M., Fally, S., Flaud, J.-M., Gamache, R. R., Goldman, A., Jacquemart, D., Kleiner, I., Lacome, N., Lafferty, W. J., Mandin, J.-Y., Massie, S. T., Mikhailenko, S. N., Miller, C. E., Moazzen-Ahmadi, N., Naumenko, O. V., Nikitin, A. V., Orphal, J., Perevalov, V. I., Perrin, A., Predoi-Cross, A., Rinsland, C. P., Rotger, M., Šimečková, M., Smith, M. A. H., Sung, K., Tashkun, S. A., Tennyson, J., Toth, R. A., Vandaele, A. C., and Vander Auwera, J.: The HITRAN 2008 molecular spectroscopic database, J. Quant. Spectrosc. Ra., 110, 533–572, 2009.

Salawitch, R. J., Weisenstein, D. K., Kovalenko, L. J., Sioris, C. E., Wennberg, P. O., Chance, K., Ko, M. K. W., and McLinden, C. A.: Sensitivity of ozone to bromine in the lower stratosphere, Geophys. Res. Lett., 32, L05811, doi:10.1029/2004GL021504, 2005.

Serdyuchenko, A., Gorshelev, V., Weber, M., Chehade, W., and Burrows, J. P.: High spectral resolution ozone absorption cross-sections – Part 2: Temperature dependence, Atmos. Meas. Tech., 7, 625–636, doi:10.5194/amt-7-625-2014, 2014.

Sioris, C. E., Haley, C. S., McLinden, C. A., von Savigny, C., McDade, I. C., McConnell, J. C., Evans, W. F. J., Lloyd, N. D., Llewellyn, E. J., Chance, K. V., Kurosu, T. P., Murtagh, D., Frisk, U., Pfeilsticker, K., Bösch, H., Weidner, F., Strong, K., Stegman, J., and Mégie, G.: Stratospheric profiles of nitrogen dioxide observed by Optical Spectrograph and Infrared Imager System on the Odin satellite, J. Geophys. Res., 108, 4215, doi:10.1029/2002JD002672, 2003.

Sioris, C. E., Kurosu, T. P., Martin, R. V., and Chance, K.: Stratospheric and tropospheric NO_2 observed by SCIAMACHY: First results, Adv. Space Res., 34, 780–785, 2004.

Sioris, C. E., McLinden, C. A., Martin, R. V., Sauvage, B., Haley, C. S., Lloyd, N. D., Llewellyn, E. J., Bernath, P. F., Boone, C. D., Brohede, S., and McElroy, C. T.: Vertical profiles of lightning-produced NO_2 enhancements in the upper troposphere observed by OSIRIS, Atmos. Chem. Phys., 7, 4281–4294, doi:10.5194/acp-7-4281-2007, 2007.

Sioris, C. E., Zou, J., McElroy, C. T., McLinden, C. A., and Vömel, H.: High vertical resolution water vapour profiles in the upper troposphere and lower stratosphere retrieved from MAESTRO solar occultation spectra, Adv. Space Res., 46, 642–650, 2010.

Thomas, R. J. and Donahue, T. M.: Analysis of Ogo 6 observations of the O I 5577-A tropical nightglow, J. Geophys. Res., 77, 3557-3565, 1972.

Toon, G., Sen, B., Blavier, J.-F., Sasano, Y., Yokota, T., Kanzawa, H., Ogawa, T., Suzuki, M., and Shibasaki, K.: Comparison of ILAS and MkIV profiles of atmospheric trace gases measured above Alaska in May 1997, J. Geophys. Res., 107, 8211, doi:10.1029/2001JD000640, 2002.

University of Saskatchewan, ftp://odin-osiris.usask.ca/Level2/no2_v6.0.2/, last access: 3 March 2017.

Vandaele, A. C., Hermans, C., Simon, P. C., Carleer, M., Colin, R., Fally, S., Mérienne, M. F., Jenouvrier, A., and Coquart, B.: Measurements of the NO_2 absorption cross-section from 42 000 cm^{-1} to 10 000 cm^{-1} (238–1000 nm) at 220 K and 294 K, J. Quant. Spectrosc. Ra., 59, 171–184, 1998.

Vicomte, M. and Pommereau, J. P.: Mini SAOZ: A Light UV-visible spectrometer sonde for studying convective transport in the stratosphere, in: Proc. 20th ESA Symposium on European Rocket and Balloon Programmes and Related Research, Hyères, France, 22–26 May 2011, ESA SP-700, 321–326, 2011.

Warshaw, G. D., Desaulniers, D.-L., and Degenstein, D.: Optical design and performace of the Odin UV/Visible spectrograph and infrared imager instrument, in: 10th Annual AIAA/USU Conference on Small Satellites, Technical Session XII: Instruments & Sensors, American Institute of Aeronautics and Astronautics (AIAA), Logan, Utah, 1996.

Weidner, F., Bösch, H., Bovensmann, H., Burrows, J. P., Butz, A., Camy-Peyret, C., Dorf, M., Gerilowski, K., Gurlit, W., Platt, U., von Friedeburg, C., Wagner, T., and Pfeilsticker, K.: Balloon-borne limb profiling of UV/vis skylight radiances, O_3, NO2, and BrO: technical set-up and validation of the method, Atmos. Chem. Phys., 5, 1409–1422, doi:10.5194/acp-5-1409-2005, 2005.

Wennberg, P. O., Cohen, R. C., Stimpfle, R. M., Koplow, J. P., Anderson, J. G., Salawitch, R. J., Fahey, D. W., Woodbridge, E. L., Keim, E. R., Gao, R. S., Webster, C. R., May, R. D., Toohey, D. W., Avallone, L. M., Proffitt, M. H., Loewenstein, M., Podolske, J. R., Chan, K. R., and Wofsy, S. C.: Science, 266, 398–404, 1994.

Wetzel, G., Bracher, A., Funke, B., Goutail, F., Hendrick, F., Lambert, J.-C., Mikuteit, S., Piccolo, C., Pirre, M., Bazureau, A., Belotti, C., Blumenstock, T., De Mazière, M., Fischer, H., Huret, N., Ionov, D., López-Puertas, M., Maucher, G., Oelhaf, H., Pommereau, J.-P., Ruhnke, R., Sinnhuber, M., Stiller, G., Van Roozendael, M., and Zhang, G.: Validation of MIPAS-ENVISAT NO_2 operational data, Atmos. Chem. Phys., 7, 3261–3284, doi:10.5194/acp-7-3261-2007, 2007.

Wetzel, G., Oelhaf, H., Kirner, O., Friedl-Vallon, F., Ruhnke, R., Ebersoldt, A., Kleinert, A., Maucher, G., Nordmeyer, H., and Orphal, J.: Diurnal variations of reactive chlorine and nitrogen oxides observed by MIPAS-B inside the January 2010 Arctic vortex, Atmos. Chem. Phys., 12, 6581–6592, doi:10.5194/acp-12-6581-2012, 2012.

Zawada, D. J., Dueck, S. R., Rieger, L. A., Bourassa, A. E., Lloyd, N. D., and Degenstein, D. A.: High-resolution and Monte Carlo additions to the SASKTRAN radiative transfer model, Atmos. Meas. Tech., 8, 2609–2623, doi:10.5194/amt-8-2609-2015, 2015.